From Waves to Watts:
A Wave Energy Conversion Device for the Charles River Basin

Matthew B. Greytak, Johanna L. Mathieu, Kathryn S. Wasserman, Anne K. Baker, Jeremy D. Chambers, and Brian M. Mueller, Massachusetts Institute of Technology.

Abstract

This paper presents the design and construction of a device that uses a linear magnetic generator to convert ocean wave energy into electrical energy. The buoyant hull of the device vertically oscillates in response to wave forcing. Within the device, a magnet is attached to a spring that is tuned to operate at resonance with respect to the dominant wave frequency. This magnet travels up and down through a coil of wire inducing a current in the coil. A data acquisition system records the voltage produced as the current in coil passes through a fixed resistive load. Based on this voltage and the value of the resistive load the power generated by the coil is calculated. This paper also presents the results of several experiments that demonstrate the functionality of this wave energy conversion device. Peak power output was measured at 36.2 mW in the Charles River Basin, Cambridge/Boston, MA. Peak efficiency was 7.30%

1. Introduction

The Massachusetts Institute of Technology Department of Ocean Engineering (Cambridge, MA) offers the courses Design of Ocean Systems I and II as the capstone design classes for undergraduate Ocean Engineering students. During the first course the students are challenged to design a system able to perform some task. The following fall they build the system they have designed. This year, the MIT Ocean Engineering undergraduate class of 2004 was challenged to:

1. Determine the power available in the wave action of the Charles River Basin, Cambridge/Boston, MA, including dependency on wind.
2. Design and construct a device to convert wave power into electrical power.
3. Measure the power output and efficiency of the wave energy converter.

This design project is especially relevant in helping promote the development of renewable and environmentally sustainable energy technologies. As the world's supply of fossil fuels diminishes and the amount of greenhouse gasses emitted into the atmosphere by anthropogenic sources increases, many researchers are exploring a variety of alternative energy sources such as hydroelectric, wind, solar, and tidal. Since the early 1970s researchers have explored the possibility of using ocean waves as a source of renewable and sustainable energy (Lewis, 1985; McCormick, 1981; Shaw, 1982). Promising designs have included the Tapered Channel, the Cockerell Raft, and the Oscillating Water Column (Clement, 2002; Climate Action Network Europe, 2004; Cockerell, 1978; Mehlum, 1991).

We began our challenge by performing background research into the many wave energy conversion devices that have been built in the past. At the same time we brainstormed new ideas for systems. In addition, we performed many laboratory experiments to test several conceptual designs. In the end the device that proved the most promising based on potential for energy extraction and ease of fabrication was a linear generator system. This paper describes the conceptual design and dynamics of our system. It also details the hull, linear generator assembly, and the electronics and data acquisition system. Next we present our experimental results and analysis. We end with a discussion of future improvements and scaling.

2. Conceptual System Design

The overall system design consists of three main components: the linear generator, the hull, and the electronics box. The linear generator assembly consists of a magnet attached to a long spring, which oscillates through an induction coil. Voltage created by the coil is measured across a 50 Ohm load resistor. The electronics measure this voltage and several sensors record the motion of the device. The hull supports the linear generator and the electronics box. Figure 1 contains a conceptual drawing of the overall system design. Each system will be discussed in more detail in the following sections. The overall design parameters were chosen based on a dynamic analysis of the system.

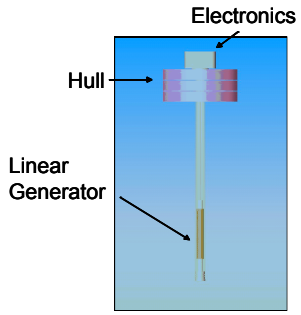

Figure 1: Conceptual design of wave energy device.

3. Dynamic Analysis

Once the basic concept of our design was in place we developed a dynamic model for the system to identify critical parameters and their effects on performance. The model was evaluated using a MATLAB script (Mathworks, Inc, www.mathworks.com).

3.1 System Model

In order to extract the most power possible from the waves we chose to excite the magnet in resonance with the waves. Systems in resonance experience a large magnitude response for a given input. In our case a magnet on a spring in resonant oscillation with the waves would have a high amplitude of oscillation, resulting in high velocities of the magnet relative to the coil. Because power from the inductor is proportional to the square of the velocity (see below), this resonant behavior was highly desired.

A system involving one spring and one mass (the magnet) is second order. A floating body also behaves like a second order system: the hydrostatic forces on the float provide an effective stiffness. The total system, with the waves as an input and the motions of the float and magnet as outputs, then becomes a fourth-order system. A dynamic model of the system is shown in Figure 2.

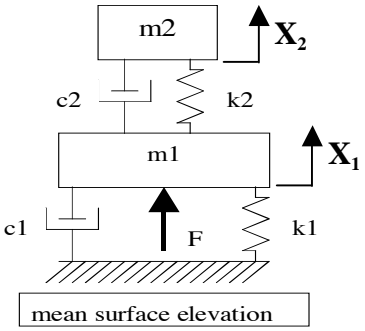

Figure 2: Dynamic model of system.

3.2 Magnet/Spring parameters

The magnet (m2) is attached to the float through an extension spring (k2). In our design the magnet slides up and down a vertical rod so that it does not bang into the coils. Bearings keep the magnet aligned on the shaft, and they contribute to a linear friction damping ($c2_{friction}$). The coils provide electromagnetic damping because energy is being removed from the mass-spring system to send power through the load resistor. This damping term (b) is described later in this paper. The total damping between the magnet and the float is then $c2 = c2_{friction} + b$.

3.3 Float parameters

The motions of floating bodies arise from static and dynamic pressures on the body surface, and viscous drag as the body moves through the fluid. The effective hydrostatic stiffness between the float's static waterline and the mean surface elevation of the waves is $k1 = \rho g A_{waterplane}$. Drag on the float arises from a combination of viscous resistance between the float and the water and wavemaking resistance as energy is expended into the surrounding water. These effects can be linearized and lumped into an effective damping term c1 which is best measured from experiment. As the float bobs in the water a certain amount of water is accelerated with the float; this added mass is combined with the mass of the float to get an effective mass m1. Added mass is also best determined experimentally.

3.4 Forcing

Pressure fluctuations underwater move the float as waves pass by. This dynamic pressure oscillation is linked to the wave elevation but the pressure fluctuations reduce with distance from the mean surface elevation. This means that bodies closer to the water surface are affected more by the waves than bodies that extend into deeper water. This is indicated mathematically:

$$p\_mag = \rho g \cdot \eta \cdot e^{kz}$$

where

p_mag = magnitude of pressure fluctuations

η = wave elevation

$k = \frac{\omega^2}{g}$ = wave number

$z \approx -$(stillwater draft)

For a sinusoidal wave of amplitude η_0 the force on the bottom of the float is:

$$F = A \cdot \rho g \cdot e^{-k \cdot draft} \cdot \eta_0 \cos \omega t$$

3.5 Transfer Functions

There are several relevant transfer functions for this system. The input to the system is the pressure force due to waves F(t) which can be computed from the wave amplitude η_0 and frequency ω from the equation above. The outputs are the position of the float x1 and the position of the magnet x2. For power production a more relevant output is the relative velocity $\dot{x}2 - \dot{x}1$. For this system the complete transfer functions are in Appendix 1.

To achieve the desired resonant behavior the magnet and spring must be tuned to the dominant wave frequency, so $k_2 = m_2\omega_{waves}{}^2$.

To get the maximum magnet response the float could be designed to be in resonance with the waves, or to be a wave follower. Experimenting with different hull parameters we found that more power could be extracted from the waves from a wave follower. To do this we made the waterplane area of the hull as large as possible while keeping the beam sufficiently small relative to the wavelength of the river waves. In the end, however, the huge amount of added mass created by our hull shape made the device more or less in tune with the waves after all. Therefore the device did not end up being a wave follower.

3.6 Dynamic Analysis Script in MATLAB

MATLAB was an ideal choice for the dynamic analysis and prediction of our system because of its Control Systems Toolbox. The transfer function tools enabled us to send an arbitrary wave into our system and predict the time-histories of the motions of the two masses. First, the parameters and equations listed in the previous sections were combined into the effective masses, springs, and dampers found in the transfer function equations. Next the forcing was calculated from the input wave and hull characteristics. The float and magnet motions were computed for a period of 10 seconds; this allowed the system to reach the steady-state. Finally the instantaneous power was calculated from the float and magnet time histories.

By adjusting the various system parameters we found that the power output is highly sensitive to the amount of mass that oscillates on the spring. More mass (requiring a stiffer spring to match the dominant wave frequency) resulted in more power output.

INPUTS	OUTPUTS
45 cm diameter hull 10 kg total mass 400 g, 1" OD, 3.2" long magnet no added mass 10% viscous damping 15% frictional damping 1 Hz wave frequency 5 cm wave amplitude 77.5 wraps per cm of coil 30 Newton magnet force	4 cm draft damped natural frequency of float is 1.92 Hz peak-to-peak magnet oscillation is 37 cm peak power output is 16 Watts RMS power output is 9 Watts

Table 1: Inputs and output of dynamics script using preliminary parameters.

The theoretical electromagnetic damping term b, the result of energy extraction from the system, was included in the mass/spring damping in early runs of the dynamic analysis script. However, later experiments with actual coils showed no signs of this term, so it was neglected.

4. Linear Generator Design and Fabrication

4.1 Theory of the Magnetic Inductance Linear Generator

The fundamental equation dictating the behavior of the linear generator is known as the Law of the Generator (Franklin *et al*, 1994). The Law of the Generator states that the voltage induced in a coil due to a moving magnet can be found from the following equation:

$V_{in} = B\, l\, v_{rel}$
where
$l = \pi\, D_{coil}\, L_m\, N$
N = # wraps / total length of coil

V_{in} in this equation is equal to the induced voltage in the coil, B is the magnetic flux of the magnet moving through the coil, D_{coil} is the outer diameter of the coil, l is the length of coil wire experiencing the flux at any given time, and v_{rel} is the relative velocity between the magnet and the coil. L_m is the total length of the magnet.

The magnetic flux in the equation above can be estimated with the following equation:

$$B = \sqrt{2 f \mu_0 / a_m}$$

where f is equal to the force of pull of the magnet, μ_o is the permeability of free space, and a_m is equal to the cross-sectional area of the magnet (Harter, 2003). The power dissipated through a load is equal to:

$P_{out} = V_{out}{}^2 / R_{load}$
where $V_{out} = V_{in} [R_{load} / (R_{coil} + R_{load})]$

The power output is maximized when the load resistor is chosen to be equal to the internal resistance of the coil.

The damping term b of the magnet's motion due to electrical energy extraction is derived as follows:

$P_{in} = v_{rel} F = v_{rel} (b v_{rel})$
$P_{out} = V_{out}^2 / R_{load} = (B^2 l^2 v_{rel}^2) / R_{load}$
$P_{in} = P_{out}$
$b = (B^2 l^2) / R_{load}$

This electromagnetic damping was imperceptible in the final apparatus, although the theory suggested that it should be quite strong. There are many possible reasons for this discrepancy, such as a saturation of the coil material or an imperfect coil. Whatever the cause, this resulted in dropping the electrical damping term from the dynamic analysis script.

4.2 Experimental Analysis

Many small coils were constructed in the initial design phases in order to gain an understanding of the generator theory. Rare earth magnets were passed through the coils as the coil output was plotted on an oscilloscope. One unexpected observation was that a spike in the voltage occurred as the magnet entered and exited the coil. It is believed that this spike in voltage is due to the entire energy in the coil being dumped to the load resistor at once. The energy in the coil is given by,

$E = 1/2 L i^2$

where L is equal to the inductance in the coil and i is the instantaneous current through the coil. As the magnet exits the coil the magnetic flux within the coil goes to zero, causing the current in the coil to go to drop to zero as well. For the current to drop to zero the energy has to be dissipated through the load resistor. Thus a spike of voltage occurs, with an associated spike in power. It is unclear whether the voltage spikes result in a larger average power than if the magnet were simply oscillating within the coil, at which time it would be operating under the law of the generator.

4.3 Linear Generator Design and Construction

The coil was wound around a 0.125"-wall acrylic tube using a homemade coil winding apparatus. The tube was rotated by a hand drill as 24-gauge magnet wire was fed onto it; a hall-effect counter kept track of the number of coil windings. The outer diameter of the final coil is 3.3 cm, with an overall length of 33 cm. The coil has four layers, with a total of 2560 wraps. A stack of 1" diameter cylindrical magnets moves on a shaft concentric to the coil. The magnet material is a machineable epoxy and neodymium-iron-born mixture which allowed us to bore out a hole for the central shaft. The final coil and magnet parameters are listed in Table 2.

Coil Parameters	Final Value
Length of Coilform	45 centimeters
Length of Coil	33 centimeters
Total Length of Wire	265.4 meters
Outer Diameter of Coil	3.3 centimeters
Number of wraps per coil length	77.5 wraps / cm
Resistance of Coil	21.5 Ω

Magnet Parameters	Final Value
Maximum Pull Force	~ 30 Newtons
Outer Diameter	2.4 centimeters
Diameter of Bore	0.95 centimeters
Total Number	8 magnets
Cumulative Length	8.13 centimeters

Table 2: Linear generator parameters.

4.4 Spring and Mass Design

The purpose of the extension spring is twofold. First, it must suspend the magnet within the coil; second, it must allow the magnet to oscillate at exactly the dominant wave frequency, or 1 Hz. The second goal is achieved simply by choosing the correct combination of spring stiffness and magnet assembly mass. To meet the first goal, the spring, magnet, and coil surround a long central shaft. The magnet rides up and down on the shaft, keeping it from hitting the sides of the coil (and thereby causing large amounts of friction). The shaft is supported between two sealed endcaps at the end of a 61" long, 2.5" OD, 2.25" ID polycarbonate tube. The coil sits in the bottom endcap and is kept in alignment with the outer tube with a disc at the top of the coil form. The overall arrangement of these components is shown in Figure 3.

In the magnet assembly a stack of eight donut-shaped magnets surrounds a central shaft; the stack remains centered and aligned due to Rulon-J sleeve bearings in the top and bottom magnets. Wrappings of lead wire increase the mass of the magnet assembly, which the dynamic analysis predicted would result in more power out of the system. The total oscillating mass is 394 grams.

The central shaft is a 0.25" diameter aluminum rod. Aluminum was chosen because it is nonmagnetic. The shaft is tensioned between the two endcaps; this keeps the shaft and magnets in sufficient alignment within the coil.

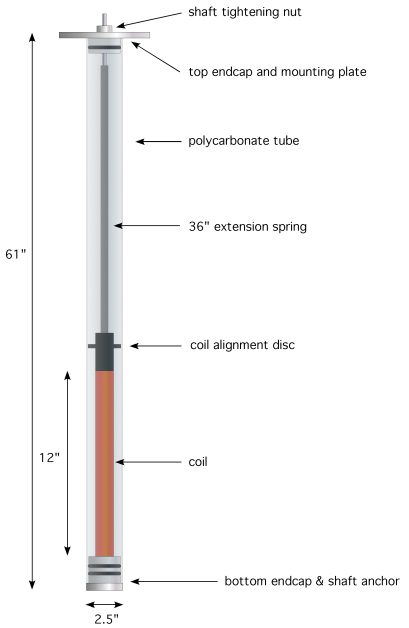

Figure 3: Linear generator tube diagram.

The necessary spring stiffness is derived directly from the oscillating mass and the dominant wave frequency using the resonance equation $k_2 = m_2\omega_{waves}^{\ 2}$. A 1 Hz natural frequency requires a fairly soft and long spring. We used a 0.5" diameter 36" long extension spring with a stiffness of 15.54 N/m to get the necessary natural frequency.

4.5 Damping

The damping ratio of the mass/spring system was measured as 8%. When the shaft was manually excited at the system's resonance the magnet moved up and down with very large oscillations. It did not take a large input amplitude to cause the mass to move so far up the shaft that it closed the spring.

5. Hull

5.1 Wave Follower

The hull is optimized for a heave response to wave motions. Its diameter of 45 cm is approximately 25% of a typical wavelength (1.6 m) of a wave in the Charles River. It floats at a draft of less than 5 cm. A rotationally symmetric shape allows the hull to respond to omnidirectional waves in the Charles.

5.2 Construction and Materials

The prototype wave power generator is made from standard, easily machinable materials to be lightweight and low-cost. The keel, which holds the linear generator, is a polycarbonate tube supported by fiberglass struts to resist bending moments. The main body is made of stacked sheets of insulation foam sandwiched between two PVC plates. The splash-proof electronics box is mounted onto the top PVC plate. A heavy electronics box mounted as high above the waterline as possible is not ideal for stability, but it allows for easy access to the electronics for maintenance. The foam provides the necessary buoyancy and the PVC plates are ideal surfaces for mounting ballast and structural components of the hull. The modular hull can be assembled or disassembled for easy transport in less than 10 minutes with only a standard Phillips-head screwdriver (see figure 4).

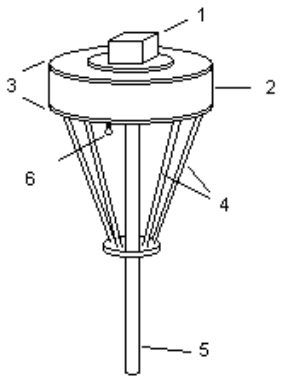

Figure 4: Basic Hull Design: 1. Electronics Box; 2. Foam Hull Body; 3. PVC Hull Plates; 4. Struts; 5. Linear Generator Housing; 6. Eye Bolt.

6. Electronics and Data Acquisition

The goal of the electronics and data acquisition system was to measure and record the power produced by the coil. Also, this system was responsible for quantifying the dynamic behavior of the device so it could be compared with the predicted behavior based on the dynamics model.

6.1 Microcomputer

The microcomputer used for data-logging was a Tattletale Model 8v2 Microcomputer (TT8) made by Onset Corporation (Bourne, MA). The TT8 is equipped with analog-to-digital (A/D) ports, time processor unit (TPU) ports, and digital ports. The TT8 has a removable Persistor Card on which data-logging computer program and data can be stored.

6.2 Power Measurement Circuit

To determine the power produced by the coil, the leads of the coil were connected to a fixed high precision load resistor (50 Ohms, rated to 0.6 Watts with a 1% tolerance). One side of this resistor was connected to analog ground and the other was connected to an analog-to-digital port of the TT8 via a signal conditioning circuit. It was necessary to condition the signal because analog-to-digital port could only handle voltages between 0 and 5 Volts. The waveform created by the coil was an irregular AC signal.

The signal was first sent through a buffer so that the signal conditioning circuit would not interfere with the behavior of the coil. Next, the gain of the signal was adjusted with an operational amplifier circuit connected for negative feedback, which therefore inverted the signal. A potentiometer was used in the gain circuit so that the gain could be easily adjusted. The signal was then added to a DC offset of 2 Volts. This DC offset inverted the signal as well. Finally, the signal was inverted one last time before being sent to the analog-to-digital port. Therefore, the output signal was centered at 2 Volts and oscillated at a magnitude set by the gain. It was also upside-down. See Figure 5 for a block diagram of the signal conditioning steps including the effective mathematical system.

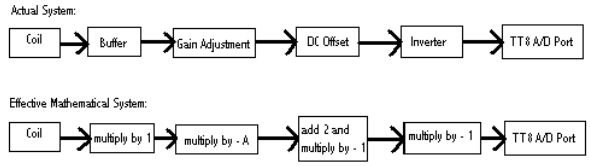

Figure 5: Block diagram of the signal conditioning steps used to convert the voltage from the coil to a signal that can enter a TT8 analog-to-digital port. Effective mathematical system is also included.

In order to minimize the volume and weight of the electronics box, and to ensure good electrical connections while in motion a printed circuit board was designed using ExpressPCB (www.expresspcb.com) software.

6.3 Sensors

Two sensor units, purchased from Crossbow (San Jose, California), were used to measure the motion of the device. An accelerometer (part number: CXL04LP1Z) measured acceleration in heave. A two-axis tilt sensor (part number: CXTA02) measured tilt in pitch and roll. This sensor also contained a temperature sensor that could be used to calibrate the tilt readings. Each of the sensor outputs—acceleration, pitch, roll, and temperature—was sent to an analog-to-digital port of our microcomputer.

6.4 Power Management

The TT8 and several LED indicator lights were powered by two 6 Volt batteries (HydriMax Ultra Rechargeable NiMH Battery Packs: 6.0 Volts, 2000mAh) wired in series to create 12 Volts. The power measurement circuitry and sensors were powered four 9 Volt batteries (Duracell Procell Alkaline Batteries: 9.0 Volts) wired in series to create +/-18 Volts, which were sent through voltage regulators to create +/-12 Volts.

6.5 Electronics Box

A 7" x 7" x 5" waterproof electronics box (with gasket) was ordered from McMaster Carr (Atlanta, GA). This accommodated all of the electrical hardware. Splash-proof connectors provided jacks for the coil, TT8 programming/communications cable, and LED indicator lights. A shorting plug on the exterior of the box was used to reset the TT8.

6.6 Data Acquisition Program

A simple data acquisition program was written in C to read data from the A/D ports hooked up to the sensors and coil. The program had three stages: initialization, sampling/writing to file, and delaying. In the initialization stage the program queries the user for the number of *samples per batch*, the *desired frequency of sampling*, and *the length of the inter-batch delay*. A sample is defined as the average of 10 A/D readings (that are taken with no time delay between them). Readings are averaged to remove some noise. A batch is a defined number of samples. The desired frequency of sampling is defined as the reciprocal of the amount of time that the program halts between taking samples. The length of the inter-batch delay is defined as the amount of time that the program halts between batches. See Figure 6 for a timing diagram.

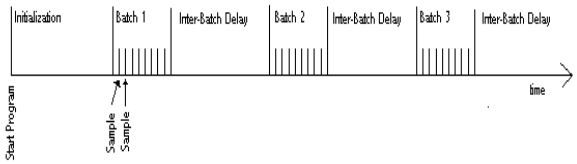

Figure 6: A timing diagram of the data acquisition program.

After initialization the program begins its second stage and starts to take data. The program takes (and writes to file) the appropriate number of samples in order to complete one batch. Since the desired frequency of sampling does not account for the amount of time taken by the program to perform its tasks the actual frequency of sampling is calculated following the completion of a batch. This value is always lower than the desired frequency of sampling. After sampling, the program goes into its third stage and delays for the length of the inter-batch delay.

6.7 Sources of Error

There are several noteworthy sources of error in the electronics that could have affected the signal measured by the TT8. First, the operational amplifiers clearly exhibited transient start-up behavior and therefore the first few data points collected were always ignored. Also, the operational amplifiers and resistors vary in their parameters as temperature, light, and humidity change. Fortunately, the most important resistors—the

load resistors—had much better specifications than normal resistors. Another source of error is the gain measurement. Undoubtedly the potentiometer controlling the gain drifted a bit with time. However, this is probably a minor error. A reasonable estimate of the total error due to the electronics is about 1 mVolt or about $2x10^{-8}$ Watts.

7. Hydrostatics and Stability

7.1 Weight Balance Spreadsheet

A weight balance spreadsheet was assembled to tabulate the weights and vertical positions of all system components with non-negligible mass. The spreadsheet calculates total weight and total submerged volume, and balances them in order to comply with Archimedes' principle and predict the hull draft.

Draft is usually defined as the depth of a ship below the waterline measured vertically to the lowest part of the hull or baseline. A more practical definition of draft for our system hull is the submerged depth of the hull above the bottom of the foam hull body, D_{WL}.

Displacement Δ	10.6061 kg
Submerged Volume	0.01061 m^3
Buoyancy Force F_B	10.6061 kg
Predicted Draft T	0.03092 m

Table 3: Weight Balance Calculations.

The predicted draft of 3 cm was observed in pool tests. After trim and ballast were added to the system hull, the observed draft was 4.5 cm.

7.2 Metacentric Stability

The spreadsheet calculates the vertical center of gravity (VCG) and the vertical center of buoyancy (VCB) for the upright stability calculations. Calculation of the longitudinal center of buoyancy (LCB) and the longitudinal center of gravity (LCG) was not justified because the transverse positions of all components were approximately on the vertical centerline. Because of the symmetry of the hull, only one metacentric height was applicable.

The center of flotation was assumed to be the geometrical center of the hull, and the assumption was validated with a re-calculation of the metacentric height for a center of flotation 5 cm from the geometrical center of the hull. The difference was less than 0.4%.

BG	0.07027 m
I_T	0.03221 m^4
BM	3.03659 m
GM_T	2.96632 m

Table 4: Metacentric Stability Results.

Spreadsheet calculations predicted positive metacentric stability, and testing confirmed these results. When the hull was given a small angle of heel, it restored itself to its upright position.

7.3 Stability at Large Angles of Heel

The righting moment at large angles of heel was calculated numerically with Hydromax software for the lightship, electronics, and magnetic generator load conditions. Several factors limit the accuracy of the Hydromax results. The unusual hullform of our system is difficult to model because MaxSurf, the solid modeling program that generates an input file for Hydromax, can model a maximum of six surfaces. Because each cylinder requires three surfaces, only two cylindrical sections of the hull could be modeled. The foam hull and the keel tube were chosen because they accounted for the most submerged volume.

maximum heel angle Φ	92.7°
maximum righting arm GZ	0.327 m

Table 5: Stability Results.

Hydromax predicted a low righting arm for the range of angles from 0° to 40°. The calculations were confirmed in pool tests when the hull barely righted itself from the maximum observed angle, and it did so very slowly.

7.4 Natural Frequency in Pitch and Roll

Roll motions were assumed to be undamped and uncoupled with pitch and heave, with non-negligible added mass. Because most of the added mass from the hull comes from the keel, the added mass calculations only account for the added mass of the keel.

Term	Definition
Roll Moment of Inertia	$I_x=(m_1z_1^2 + m_2z_2^2 + m_3z_3^2 + m_nz_n^2)$
Radius of Gyration	$k_x = \mathrm{sqrt}(I_x/M)$
Added Mass Moment of Inertia	$I_{am} = (\pi D^2)(r_{end}^3-r_0^3)/12$
Natural Frequency	$\omega = gGM/(1+x_a)k_x^2$

Table 6: Terms and Definitions.

Roll Moment of Inertia	3.6064 kgm^2
Radius of Gyration	0.5831 m
Natural Frequency	6.9241 rad/sec
Natural Frequency	1.1020 Hz

Table 7: Natural Frequency Calculations.

The observed natural frequency in roll during pool tests was approximately 1 Hz.

8. Experimental Design and Experimentation

8.1 Preliminary Testing

After thoroughly testing each subsystem in the laboratory the entire system was tested at the MIT Zesiger Sports and Fitness Center pool on November 16, 2003. The purpose of the pool test was to determine basic structural integrity, to test waterproofing, to ballast and trim the hull, and to evaluate system integration including the electronics. A goal of the test was to log sensory data and measure voltage from coil in three testing situations: when the hull was forced up and down in the water, when the hull was floating freely, and when artificial waves were induced near the hull. After ballasting to level trim the draft was 4.5 centimeters. The period in pitch and roll was 3.84 seconds, and the heave period was 0.98 seconds. The heave oscillations were observed to be very strongly damped.

8.2 Field Testing

On November 20 2003, the entire system was tested in its designed operating environment in the Charles River off the MIT Sailing Pavilion dock. The trim was level and the draft was observed to be 4.5 cm, so no additional ballast or trim was added. The temperature was 7.22° C and the wave heights were observed to be 1 cm to 3 cm peak-to-peak, with periodic ripples from the wind. The windspeed was approximately 5 knots.

In order to determine the total power available in the waves and, subsequently, the efficiency of our device, several homemade wave probes were deployed concurrently. These probes measured wave height using a conductance method (Chen, 1994). The data from this deployment was found to be invalid, so the wave probes were re-deployed approximately half an hour after deployment of the power-generating device. Thus there is no direct time correlation between the wave probe data and the system sensor and power data, but the wave probe data accurately describes the sea state in which the system was deployed. Another set of system data was logged on the opposite side of the river where the waves were observed to be larger, but no wave probe data was logged on that side of the river to correlate with the system data.

9. Power and Efficiency Results

9.1 Data Processing

In order to process the power data, we performed a series of calculations to convert the A/D readings to Volts. To calculate power in Watts each voltage was then squared and divided by 50 Ohms, the value of the resistive load. Also, RMS voltage and power were computed from the voltage data to give us an idea of how much DC voltage might be derived from our waveform.

9.2 Processed Voltage/Energy Data

Figure 7 shows a plot of a small section of the post-processed voltage data from the pool test. This data was recorded as the device responded to manmade waves. Much of the good data from both the pool and river tests looks like this. The peak voltage is defined as the highest absolute value the coil achieves (in this case ~1350 mVolts). The peak power is this voltage squared and divided by 50 Ohms. The RMS voltage and power were calculated from the individual samples. Figure 8 shows the power calculated from these voltage measurements over the same time span.

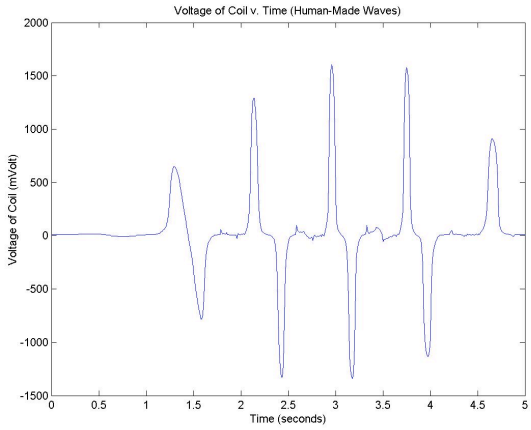

Figure 7: Plot of a small section of the post-processed voltage data from the pool test.

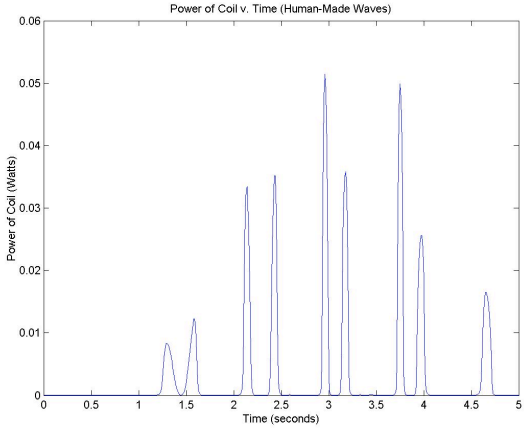

Figure 8: Plot of the power computed from the voltage data presented above.

Table 8 shows some sample data. This data was collected while the device operated in the river a few feet from the wave probes and was used for calculating the efficiency of the device.

Batch No.	Peak Voltage (mV)	Peak Power (mW)	RMS Voltage (mV)	RMS Power (mW)
6	436.667	3.8136	53.1063	0.0564
7	393.95	3.1039	72.3599	0.1047
8	326.325	2.1298	53.0165	0.0562
9	124.713	0.3111	19.6471	0.0077
10	26.4408	0.0140	6.53389	0.0009
11	265.543	1.4103	38.0181	0.0289
12	314.957	1.9840	37.6149	0.0283
13	38.3761	0.0295	7.31125	0.0011

Table 8: Sample results from river testing.

9.3 Wave Probe Results

The results from our wave probes, which successfully collected wave data a short time after the wave energy conversion device had been operating in the waves, are presented in Table 9.

Significant Wave Height	0.01756 m
Total Energy	0.1910 J/m
Peak Frequency	1.405 Hz
Peak Wavelength	0.791 m
Peak Period	0.712 s
Total Power	0.1155 W/m

Table 9: Wave probe data.

The peak frequency of the waves (1.41 Hz) was higher than that designed for — 1Hz. The significant wave height matches observation.

9.4 Power Results

The data presented in Table 8 shows that under small wave conditions, which it experienced while it operated near the dock, the peak power is only 3.81 mW and its average RMS power is 0.0355 mW. The peak value jumps up to 36.2 mW and the average RMS value jumps up to 0.096mW when the device was in the middle of the river. In the pool, the human-made waves were probably the largest and most regular that the device saw. The peak power there was 57.9 mW and average RMS value was 1.4519 mW. This is similar to the highest values that we saw in lab by shaking the device — 62 mW.

9.5 Efficiency Results

The wave probes show that the power in the waves was 0.1155 W/m. Since our device is 0.45 meters the total wave power our device saw at any one time was .0522 W/m. Therefore, the maximum efficiency of our wave energy conversion device was 7.30%. The average RMS efficiency was 0.068%.

9.6 Dynamic Results

Accelerometer and tilt sensor data were collected at 32 Hz during the river testing. Each sensor data point is the result of averaging ten collected data points, so no further data filtering was required. Even though the waves in the river on the test day were at a frequency of 1.41 Hz, the heave acceleration data has a frequency peak at 0.95 Hz. The pitch and roll data show a peak around 1 Hz as well; this is most likely a coupling effect with the heave motions. However they have another peak around 0.25 Hz which corresponds with the measured roll natural frequency from pool testing.

9.7 Update to Dynamics Model

The "experimentally determined" parameters of the dynamics model such as added mass and viscous/wavemaking resistance were estimated from the pool test results. The viscous damping ratio was around 60%. The heave natural frequency measured at the pool was 0.98 Hz. The hydrostatic stiffness of the float was 1560.2 N/m, so the total oscillating mass in the heave natural frequency test must have been 26.34 kg. The added mass was therefore the total oscillating mass minus the mass of the float and magnet, or 26.34 kg – 10.212 kg – 0.394 kg = 15.73 kg added mass. These parameters, along with the actual wave conditions on the river from the test day, were entered back into the dynamic analysis script to compare predicted power output to actual power output. The results are listed in Table 10.

Dynamics Script Prediction Using Measured Wave Parameters	Measured Performance (where wave probe data is available)
Float damped natural frequency = 0.98 Hz Peak acceleration = 0.04 g Peak output power = 113 mW RMS power output = 67 mW	Heave acceleration frequency = 0.95 Hz Peak acceleration = 0.05 g Peak output power = 3.8 mW RMS output power = 0.04 mW

Table 10: Comparison of actual performance with predicted performance.

The device did not respond at the wave frequency, as the dynamics equations and linear theory predicted that it would. Instead it responded very close to the damped natural frequency of the device. That means that the waves acted more like impulses, setting the float into free oscillation, rather than behaving like a continuous forcing and pulling the float along at the wave frequency. That is most likely due to the irregular nature of the waves.

10. Discussion

10.1 Improvements to the Design

There are several changes that would greatly improve the performance of the device. The device could be made into a wave follower by decreasing the diameter of the hull and the weight of the device. Unfortunately, decreasing the diameter of the hull would decrease its stability. With a smaller hull, it would be important to lower the electronics box, perhaps imbedding it within the foam hull. The linear generator could also be greatly improved. With a better understanding of linear generator theory, the dimensions of the coil could be optimized. Additionally, a much stronger magnet could be used, and the load resistor could be optimized to have the same resistance as the coil. This would allow a much larger power output than the current design. Lastly, the spring could be dynamically adjusted to tune the mass-spring system to resonate at the exact same frequency as the hull. This would be a very complicated task, but it would make the device effective over a large range of sea states.

10.2 Scaling

The wave power device could be used in most any location. However, the mass-spring system would need to be tuned to resonate at the peak frequency of the waves. In a larger basin, such as the ocean, the device could not be in resonance with the waves, because the peak frequency is much too low; it would require a prohibitively long spring to resonate at that frequency. The device would need to be designed to respond at a frequency much higher than the peak frequency of ocean waves. Ocean waves, however, occur over such a broad range of frequencies and so the device could still be effective. How effective, though, is yet to be determined. More research needs to be done into linear generator theory in order to know exactly how the device would perform on a larger scale.

11. Conclusion

This paper has presented the theory and design for a wave energy device with uses a linear generator to derive power from the motion of river waves. The device has been designed to operate in the Charles River Basin but could be modified for operation in the Ocean. Research into wave energy devices is important in the promotion of renewable energy in light of dwindling supplies of fossil fuel sources and global climate change accelerated by anthropogenic activities.

References

Chen, D.J., Designing Wave Measuring Instruments. Thesis, MIT Dept. of Ocean Engineering: 1994.

Clement, A. et al., "Wave Energy in Europe: Current Status and Perspectives." Renewable and Sustainable Energy Reviews. Vol 6. pp405-431. Pergamon Publishing: 2002.

Cockerell, C. et al, "The Development of the Wave-Contouring Raft." Proceedings of the Wave Energy Conference, London-Heathrow: 1978.

Climate Action Network Europe, "Further Information on Wave Energy." www.climnet.org/EUenergy/wave.html. 2004.

Franklin, G. et al, Feedback Control of Dynamic Systems, Third Edition, Addison-Wesley: 1994.

Harter, J., Electromechanics: Principles, Concepts, and Devices. Pearson Education: 2003.

Lewis, T. Wave Energy: Evaluation for the C.E.C. Graham Trotman: 1985.

Mehlum, E., "Commercial Tapered Channel Wave Power Plants in Australia and Indonesia." Proceedings of OCEANs, Honolulu, Hawaii: 1991.

McCormick, M.E., Ocean Wave Energy Generation. Wiley and Son: 1981.

Shaw, R., Wave Energy: A Design Challenge. Ellis Horwood Ltd: 1982.

Acknowledgements

The MIT Ocean Engineering class of 2004 would like to thank our 13.017/13.018, Design of Ocean Systems I and II course instructors: Dr. Thomas Consi, Dr. Franz Hover, and Prof. Michael Triantafyllou. In addition we would like to thank Prof. Steven Leeb in the MIT Electrical Engineering and Computer Science Department; and Fran Charles at the MIT Sailing Pavilion.

Appendix 1: Complete system transfer functions for hull dynamics model.

$$\frac{X_1}{F} = \frac{m_2 s^2 + c_2 s + k_2}{m_1 m_2 s^4 + \left(m_1 c_2 + m_2 \left(c_1 + c_2\right)\right) s^3 + \left(m_1 k_2 + m_2 \left(k_1 + k_2\right) + c_1 c_2\right) s^2 + \left(c_1 k_2 + c_2 k_1\right) s + k_1 k_2}$$

$$\frac{X_2}{F} = \frac{c_2 s + k_2}{m_1 m_2 s^4 + \left(m_1 c_2 + m_2 \left(c_1 + c_2\right)\right) s^3 + \left(m_1 k_2 + m_2 \left(k_1 + k_2\right) + c_1 c_2\right) s^2 + \left(c_1 k_2 + c_2 k_1\right) s + k_1 k_2}$$

$$\frac{X_2}{X_1} = \frac{c_2 s + k_2}{m_2 s^2 + c_2 s + k_2}$$

$$\frac{\text{rel. velocity}}{F} = \frac{s\left(X_2 - X_1\right)}{F} =$$

$$= \frac{-m_2 s^3}{m_1 m_2 s^4 + \left(m_1 c_2 + m_2 \left(c_1 + c_2\right)\right) s^3 + \left(m_1 k_2 + m_2 \left(k_1 + k_2\right) + c_1 c_2\right) s^2 + \left(c_1 k_2 + c_2 k_1\right) s + k_1 k_2}$$